Published in final edited form as:

Hippocampus. 2023 April ; 33(4): 424–441. doi:10.1002/hipo.23505.

Neuroligin-2 controls the establishment of fast GABAergic transmission in adult-born granule cells

Ayelén I. Groisman[*],
Andrea Aguilar-Arredondo[*],
Damiana Giacomini,
Alejandro F. Schinder

Laboratorio de Plasticidad Neuronal, Fundación Instituto Leloir, Av. Patricias Argentinas 435, C1405BWE – Buenos Aires, Argentina

Abstract

GABAergic inhibition is critical for the precision of neuronal spiking and the homeostatic regulation of network activity in the brain. Adult neurogenesis challenges network homeostasis because new granule cells (GCs) integrate continuously in the functional dentate gyrus. While developing, adult-born GCs undergo a transient state of enhanced excitability due to the delayed maturation of perisomatic GABAergic inhibition by parvalbumin interneurons (PV-INs). The mechanisms underlying this delayed synaptic maturation remain unknown. We examined the morphology and function of synapses formed by PV-INs onto new GCs over a 2-month interval in young adult mice, and investigated the influence of the synaptic adhesion molecule neuroligin-2 (NL2). Perisomatic appositions of PV-IN terminals onto new GCs were conspicuous at 2 weeks and continued to grow in size to reach a plateau over the 4th week. Postsynaptic knockdown of NL2 by expression of a short-hairpin RNA (shNL2) in new GCs resulted in smaller size of synaptic contacts and reduced area of perisomatic appositions of the vesicular GABA transporter VGAT. GCs expressing shNL2 displayed spontaneous GABAergic responses with decreased frequency and amplitude, as well as slower kinetics compared to control GCs. In addition, postsynaptic responses evoked by optogenetic stimulation of PV-INs exhibited slow kinetics, increased paired-pulse ratio and coefficient of variation (CV^2) in GCs with NL2 knockdown, suggesting a reduction in the number of active synapses as well as in the probability of neurotransmitter release (P_r). Our results demonstrate that synapses formed by PV-INs on adult-born GCs continue to develop beyond the point of anatomical growth, and require NL2 for the structural and functional maturation that accompanies the conversion into fast GABAergic transmission.

Correspondence should be addressed to: aschinder@leloir.org.ar or dgiacomini@leloir.org.ar.
(*)Equally contributing authors

CONFLICT OF INTEREST
The authors declare that they have no competing interests.

Keywords

adult neurogenesis; dentate gyrus; excitability; interneurons; neural development; synaptogenesis; plasticity

1 INTRODUCTION

In all mammals, including humans, adult neurogenesis occurs in the dentate gyrus resulting in an increase in the degree of plasticity of the hippocampal circuit (Goncalves, Schafer, & Gage, 2016; Mongiat & Schinder, 2011; Moreno-Jimenez et al., 2019; van Praag et al., 2002). This remarkable circuit remodeling is critical for learning and for the generation of long-term memories. While developing, adult-born granule cells (GCs) are stimulated by the surrounding network and, in particular, by the activity of GABAergic interneurons that promote their growth and maturation (Trinchero, Giacomini, & Schinder, 2021). Thus, GABAergic signaling promotes early differentiation and survival of neural stem cells and their neuronal progeny (Song et al., 2013; Song et al., 2012). As new GCs develop, they receive depolarizing GABAergic transmission that promotes maturation and circuit integration (Alvarez et al., 2016; Chancey et al., 2013; Ge, Yang, Hsu, Ming, & Song, 2007; Heigele, Sultan, Toni, & Bischofberger, 2016; Remmers, Castillon, Armstrong, & Contractor, 2020; Song et al., 2013). Those early postsynaptic responses exhibit immature features such as small conductance and slow kinetics that, combined with the incoming glutamatergic inputs, produce a high excitation/inhibition balance that results in a transient period of increased excitability and plasticity (Dieni et al., 2016; Ge et al., 2007; Lodge, Hernandez, Schulz, & Bischofberger, 2021; Marin-Burgin, Mongiat, Pardi, & Schinder, 2012). Therefore, such enhanced excitability is most likely consequence of the delayed maturation of perisomatic inhibition in newborn GCs (Groisman, Yang, & Schinder, 2020).

Inhibitory networks control the activity and rhythm of principal neurons in the brain through specialized chemical synapses that depend on specific intracellular and transsynaptic scaffolds. In the dentate gyrus, the local excitation/inhibition balance of principal cells is mainly controlled by parvalbumin- (PV-INs) and somatostatin-expressing interneurons (SST-INs) (Hosp et al., 2014; Kepecs & Fishell, 2014). These INs control different subcellular domains of GCs, with PV-INs reaching the granule cell layer (GCL) and contacting the soma, and SST-INs targeting the dendrites in the molecular layer (Groisman et al., 2020; Yuan et al., 2017). In newborn GCs, initial functional contacts by PV-INs and SST-INs become detected between the first and the second week of development and increase in number during the following weeks upon reaching maximal levels of inhibition with both fast kinetics and large conductance by 6–8 weeks, as revealed by optogenetic activation in acute slices (Groisman et al., 2020; Lodge et al., 2021; Remmers et al., 2020; Vaden et al., 2020).

Although GABAergic inputs are restricted to distinct cellular compartments, similar protein complexes assemble an orchestrated code to organize inhibitory synapses (Ali, Marth, & Krueger-Burg, 2020; Yogev & Shen, 2014). The neuroligin (NL) family stands out as a crucial player in the postsynaptic density by promoting the assembly of presynaptic release

sites (Huang & Scheiffele, 2008). In particular, neuroligin-2 (NL2) is essential for the correct specification of GABAergic perisomatic synapses, and its deletion may produce a selective decrease in perisomatic inhibitory postsynaptic currents (IPSCs) across brain regions (Chanda, Hale, Zhang, Wernig, & Sudhof, 2017; Chubykin et al., 2007; Poulopoulos et al., 2009; Varoqueaux et al., 2006; Zhang et al., 2015). In line with these observations, $NL2^{-/-}$ mice show increased excitability in mature GCs that is associated to a reduction in the levels of gephyrin and the gamma2 subunit of the $GABA_A$ receptor specifically in the perisomatic region (Jedlicka et al., 2011). Conversely, overexpression of NL2 increases the density of VGAT-containing terminals on the soma of newly generated GCs (Krzisch et al., 2016). Moreover, the altered expression or mutations in NL2 are linked to cognitive and psychiatric disorders, including schizophrenia, autism and anxiety (Ali et al., 2020).

The coupling of adult-born GCs to the inhibitory network represents the final step in their functional integration and the establishment of fast perisomatic transmission is most likely what determines the switch from high excitability to sparse activation that is characteristic of mature GCs (Trinchero et al., 2021). The mechanisms underlying such delayed maturation of the PV-IN to GC synapse remain unknown. Here, we characterized the morphological development of the synapse between PV-INs and new GCs and found that synaptic size increases during the initial 4 weeks, with no further changes at later time points, although functional transmission continues beyond this point. Remarkably, NL2 knockdown produced a substantial reduction in the size of mature perisomatic contacts, decreased the number of functional synaptic contacts and the remaining synapses failed to achieve functional maturation as revealed by electrophysiological recordings. Our results unravel NL2 as a crucial player for the maturation of fast inhibition in developing GCs of the adult hippocampus.

2 MATERIALS AND METHODS

2.1 Mice

Experimental protocols were approved by the Institutional Animal Care and Use Committee of the Leloir Institute according to the Principles for Biomedical Research involving animals of the Council for International Organizations for Medical Sciences and provisions stated in the Guide for the Care and Use of Laboratory Animals. C57Bl/6J and transgenic mice of either sex (5 – 7 weeks of age) were housed at four to five mice per cage in standard conditions. Genetically modified driver mice $Pvalb^{Cre}$ ($Pvalb^{tm1(cre)Arbr/J}$), kindly provided by S. Arber (Hippenmeyer et al., 2005, and $CAG^{floxStop\text{-}tdTomato}$ (Ai14) ($B6;129S6\text{-}Gt(ROSA)26Sor^{tm14(CAG\text{-}tdTomato)Hze/J}$) conditional reporter line (Madisen et al., 2010), were crossed to generate $PV^{Cre};CAG^{floxStop\text{-}tdTomato}$ mice to label PV-expressing GABAergic interneurons with tdTomato (tom). $Pvalb^{Cre}$ mice were also crossed with $CAG^{floxStopChR2\text{-}EYFP}$(Ai32) ($Gt(ROSA)26Sor^{tm32(CAGCOP4*H134R/EYFP)Hze/J}$) mice from Jackson Laboratories, to generate $PV^{Cre};CAG^{FloxStopChR2}$ mice for optogenetic experiments. Mice were maintained in C57BL/6J background.

2.2 Production of viral vectors

A replication-deficient retroviral vector based on the Moloney murine leukemia virus was used to specifically transduce adult-born GCs as done previously (Temprana et al., 2015). Retroviral particles were assembled using three separate plasmids containing the capsid (CMV-vsvg), viral proteins (CMV-gag/pol) and the promoter-transgenes cassette: CAG-GFP, U6-shNL2-CAG-GFP, U6-shScramble (SCR)-CAG-GFP or Ubi-channelrhodopsin-2-GFP (Ubi-ChR2-GFP, kindly provided by S. Ge, SUNY Stony Brook). Plasmids were transfected onto HEK 293T cells using deacylated polyethylenimine. HEK 293T cells were cultured in Dulbecco´s Modified Eagle´s Medium with high glucose, supplemented with 10 % fetal calf serum and 2 mM glutamine. The virus-containing supernatant was harvested 48 h after transfection and concentrated by two rounds of ultracentrifugation. Virus titer was typically ~10^5 particles/µl.

To generate the retrovirus expressing shNL2-GFP, the U6 promoter-shNL2 cassette was subcloned from the pLenLox_U6 Nlgn2 plasmid (gift from Peter Scheiffele; Addgene plasmid # 59358) (Chih, Engelman, & Scheiffele, 2005) using standard PCR-based techniques. The primers used were: 5'-ATCGATGATCCGACGCGCCATCTCTAG-3' (primer U6-shNL2 forward), 5'-ATCGATGAAAAAAGGAGCAAGTTCAACAGCAATC-3' (primer U6-shNL2 reverse). The full-length fragment was then subcloned by ClaI into the original CAG-GFP retroviral plasmid. For the generation of the shSCR plasmid, the online tool (https://www.invivogen.com/sirnawizard/scrambled.php) was used and the original shNL2 sequence was replaced by 5'-GCAGGAACAACCGAGTAATTTCAAGAGAATTACTCGGTTGTTCCTGC-3'.

2.3 Stereotaxic surgery for retroviral delivery

Running wheel housing started 2-3 days before surgery and continued until the day of slice preparation or brain fixation, to maximize the number of retrovirally transduced neurons. For surgery, mice were anesthetized (150 µg ketamine/15 µg xylazine in 10 µl saline/g), and retrovirus was infused into the dorsal region of the right dentate gyrus (1-1.5 µl at 0.15 µl/min) using sterile calibrated microcapillary pipettes through stereotaxic references. Coordinates from bregma (mm): −2 anteroposterior, −1.5 lateral, −1.9 ventral. A single injection site was sufficient to label a sufficient number of neural precursor cells. Animals were killed 6 weeks post infection (wpi) for immunofluorescence or electrophysiological recordings.

2.4 Slice preparation

Mice were anesthetized and decapitated at 6 wpi as indicated, and transverse slices were prepared as described previously (Marín-Burgin et al., 2012). Briefly, brains were removed into a chilled solution containing (in mM): 110 choline-Cl^-, 2.5 KCl, 2.0 NaH_2PO_4, 25 $NaHCO_3$, 0.5 $CaCl_2$, 7 $MgCl_2$, 20 glucose, 1.3 Na^+-ascorbate, 0.6 Na^+-pyruvate and 4 kynurenic acid. The hippocampus was dissected, and transverse slices of septal pole (400 µm thick) were cut in a vibratome and transferred to a chamber containing artificial cerebrospinal fluid (ACSF; in mM): 125 NaCl, 2.5 KCl, 2 NaH_2PO_4, 25 $NaHCO_3$, 2 $CaCl_2$, 1.3 $MgCl_2$, 1.3 Na^+-ascorbate, 3.1 Na^+-pyruvate, and 10 glucose (315 mOsm). Slices

were bubbled with 95% O_2/5% CO_2 and maintained at 32°C for at least 1 hour before experiments started.

2.5 Electrophysiology

Whole-cell recordings were performed in ACSF containing APV 100 μM + DNQX 20 μM (a few experiments were instead done with kynurenic acid 4 mM), at room temperature (23±2°C) using microelectrodes (4-6 MΩ) filled with internal solution. Two internal solutions were used that contained (in mM): EGTA 0.1, Hepes 10; Tris-ATP 4; Tris-GTP 0.3; phosphocreatine 10; and Alexa Fluor 594 (10 $\mu g.ml^{-1}$; Invitrogen), pH 7.3 and 290 mOsm. To measure sIPSCs we included (in mM): CsCl 140; NaCl 5; $MgCl_2$ 2; EGTA 0.1. To measure eIPSCs we included (in mM): 110 K-gluconate, 5 NaCl, 30 KCl and 4 $MgCl_2$. All chemicals were from Sigma. All recordings were obtained using patch clamp amplifiers, digitized, and acquired at 10-20 KHz onto a personal computer. Membrane capacitance and input resistance were obtained from current traces evoked by a hyperpolarizing step (10 mV, 100 ms) and $V_{HOLDING} = -70$ mV.

Adult-born GCs expressing GFP, shNL2-GFP or SCR-GFP were visually identified in the GCL by fluorescence (FITC fluorescence optics) and infrared videomicroscopy. Criteria to include cells in the analysis were visual confirmation of fluorescent protein in the pipette tip, attachment of the labeled soma to the pipette upon negative pressure, and absolute leak current <100 pA at $V_{HOLDING}$ for GCs. Unlabeled neurons localized in the outer third of the GCL were selected here as unlabeled mature controls (Laplagne et al., 2006). As in previous studies, we took advantage of the reversal potential of GABA-mediated IPSCs (E_{GABA}) to determine the subcellular origin of GABAergic inputs (Groisman et al., 2020; Laplagne et al., 2006). This approach allowed to discriminate proximal and distal GABAergic currents in the same neurons.

2.6 Optogenetics and electrical stimulation

Patch-clamp recordings were carried out in adult-born GCs from hippocampal slices containing PV-INs expressing ChR2(Groisman et al., 2020). The latter were visualized by their EYFP expression. PV-INs were stimulated with laser pulses (0.2 ms, power intensity < 100 mW) using a 447 nm source delivered through the epifluorescence pathway of the upright microscope (FITC filter, 63X objective), commanded by the acquisition software. Outer molecular layer (OML) stimulation was performed by placing a steel monopolar electrode in the outer third of the molecular layer, >300 μm away from the recording site. Current pulses ranging from 40 to 100 μA (0.2 ms) were applied at 0.07 Hz in the presence of glutamate receptor blockers to activate GABA release onto distal dendrites.

2.7 Data analysis

Spontaneous IPSCs were sampled for >5 minutes, digitally filtered at 1 kHz, and detected offline with Mini Analysis software (Synaptosoft, [https://minianalysis.software.informer.com/]). For analysis, a low-pass Butterworth filter was applied with a cut-off frequency of 500 Hz. The amplitude and area thresholds for detection were 10 pA and 50 pA.ms. All events were individually validated, and artifacts were discarded by visual inspection. Rise time was measured from 10 to 90% of the peak

amplitude. Only cells with >30 events were considered for analysis. The median of the rise time distribution and of the peak amplitude was obtained for each cell.

Evoked IPSCs were analyzed with Clampfit software. Rise and decay times were calculated from 20 to 70% and from 70 to 30 % of peak amplitude, respectively. The coefficient of variation (CV^2) was calculated as the squared ratio of the standard deviation and the mean of the eIPSC amplitudes. For train stimulation, the normalized total charge was calculated as the charge of the entire eIPSC over 350 ms and normalized to the peak amplitude. The paired pulse ratio was measured as the peak amplitude of each individual pulse response and normalized to the first pulse of each train.

2.8 Immunofluorescence

Immunostaining was performed in 40 μm-thick free-floating coronal sections throughout the septal fraction of the hippocampus from $PV^{Cre};CAG^{floxStop\text{-}tdTomato}$ mice. Slices were exposed to citrate buffer for antigen retrieval and washed 3 times for 5 minutes at 65°C. Antibodies were applied in TBS with 3% donkey serum and 0.25% Triton X-100. Triple labeled immunofluorescence was performed using the following primary antibodies: GFP (Chicken antibody IgY Fraction 1:500, Aves Labs Inc.), RFP (rabbit or goat anti-RFP polyclonal antibody, 1:500, Rockland) and VGAT (rabbit-anti VGAT polyclonal antibody 1:250, Synaptic Systems). The RFP antibody was used for optimal detection of Tom reporter protein. The following corresponding secondary antibodies were used: donkey anti-chicken Cy2 or Cy5, donkey anti-rabbit Cy5 and donkey anti-rabbit or mouse Cy3, (1:250; Jackson ImmunoResearch Laboratories). Incubation with DAPI (10 minutes) for nuclear counterstain was applied to avoid fluorescent bleaching when slice characterization was performed. Slices were mounted and covered with gerbatol to prevent bleaching.

2.9 Confocal Microscopy

Sections from the septal hippocampus according to the mouse brain atlas (antero-posterior, −0.94 to −2.46 mm from bregma) were included (Paxinos & Franklin, 2001). Images were acquired using Zeiss LSM 710 NLO and 880 LSM Airyscan microscopes (Carl Zeiss, Jena, Germany). Analysis of antibody expression was restricted to cells with fluorescence intensity levels that enabled clear identification of their soma. Images were acquired (63X, NA 1.4, oil-immersion, digital zoom 7x) and colocalization for the two markers (GFP and tom, or GFP and VGAT) was assessed in z-stacks including 25-35 optical slices for each soma (airy unit=1 at 0.25 μm intervals).

Images were analyzed using the colocalization module of ZEN Pro 3.3 software (Zeiss, Germany) to detect and quantify area of colocalization of two channels in the image. First, the image was manually processed plane-by-plane to delimit the region of the GC soma, corresponding to one channel in the entire 3-D projection. A z-stack projection of all optical slices was obtained, and a ROI was traced around the perimeter of the GC soma. Then, the second channel was processed to subtract the labeling outside the ROI demarcating the GC soma. Finally, the area of the entire soma and the region of colocalization were measured. The analysis included 29 to 85 neurons per condition.

3 RESULTS

Perisomatic GABAergic transmission can be detected within the first days of development in adult-born GCs, and it is primarily conveyed by PV-INs (Song et al., 2013; Vaden et al., 2020). Still, these synapses only become functionally mature after >6 weeks (Groisman et al., 2020). To determine whether this slow developmental timing is consequence of a protracted synaptogenesis or whether it is due to a delayed functional maturation of established contacts, we first characterized perisomatic synaptogenesis at the morphological level using confocal imaging. GCs generated in the adult dentate gyrus were labeled using retroviruses expressing GFP (RV-ChR2-EGFP or RV-GFP, as indicated), and PV-INs were labeled in PV^{Cre};$CAG^{floxtdTomato}$ mice (aging 6 – 7 weeks) (Groisman et al., 2020; Temprana et al., 2015). Projections expressing tdTomato (Tom) were clearly visible, intermingled within the GCL and surrounding the cell bodies (Fig. 1A). PV-IN axons and somas of mature adult-born GC displayed multiple sites of overlap within the GCL, consistent with putative synaptic sites. Indeed, immunostaining for the vesicular GABA transporter VGAT displayed punctate signals surrounding the somas throughout the GCL (Fig. 1B). Detailed analysis of adult-born GCs revealed PV-IN terminals colocalizing with VGAT in multiple sites around the soma (Fig. 1C). The overlap between PV-Tom and VGAT signals indicates that Tom^+ axons enclosing GABA-containing vesicles are presynaptic boutons from PV-INs reaching the soma of labeled GCs (Fig 1D)(Chaudhry et al., 1998; Crosby et al., 2019; Fritschy & Panzanelli, 2014).

To learn about the timing of structural synaptogenesis, we monitored the size of PV-Tom contacts formed onto developing GCs at 2-, 4- and 8-weeks post infection (wpi)(Fig. 2A). Three-dimensional reconstructions of individual GC somas were obtained by confocal imaging to measure the projected area of the cell bodies and the overlay between PV-IN axons and the GC surface (Fig. 2B,C). The projected soma was approximately 90 μm^2 for neurons at 2 and 4 weeks, and decreased slightly at 8 weeks (Table 1). We observed clear appositions between PV axons and GC somas already at 2 weeks, although the majority of those contacts displayed small colocalization area (Fig. 2D). At this age, the mean synaptic area was approximately 5 μm^2, which corresponded to a proportion of ~6 % of the projected surface of the soma (Fig. 2C,D; Table 1). At 4 weeks, all neurons showed conspicuous perisomatic labeling, with contacts in the range of 5 to 25 μm^2, with an average area near 13 μm^2. Because functional inhibition matures substantially after 4 weeks (Groisman et al., 2020), we reasoned that the size of perisomatic contacts might experience further growth at later times. However, somatic appositions displayed no further growth at 8 weeks, indicating that the plateau level had been reached at 4 weeks, and functional changes beyond that point might arise from the maturation of preexisting structural contacts (Fig. 2C,E).

The involvement of NL2 in perisomatic appositions targeting new GCs was analyzed at 8 wpi using a retrovirus expressing a shRNA to knockdown NL2 (RV-shNL2-GFP), or a control virus expressing a scrambled shNL2 sequence (RV-SCR-GFP) (Fig. 2F). Eight-week-old GCs developing under chronic expression of shNL2 displayed normal overall morphology and dendritic tree length, along with intrinsic functional parameters (Table 1). However, a slight reduction of the soma size together with an increased membrane resistance suggest that NL2 knockdown keeps new GCs from reaching fully mature characteristics at

the time of observation. The most prominent feature of GCs expressing shNL2 was a 50 % reduction in the overlap area of PV-Tom terminals when compared to those expressing SCR, which showed similar size as control GCs (Fig. 2G,H; Table 1). To further investigate whether NL2 knockdown may be interfering with synapse formation, we measured the area of VGAT. GCs expressing shNL2 displayed a substantial reduction in the area of somatic VGAT labeling, similar in magnitude to the effect observed in PV-Tom terminals (Fig. 2 I,J). These results reveal a critical role for NL2 in perisomatic synaptogenesis onto newborn GCs.

To investigate if the structural alterations induced by shNL2 are mirrored by functional modifications, the effects of NL2 knockdown were assessed by whole-cell recordings carried out in acute slices. To discriminate perisomatic (proximal) from dendritic (distal) responses, spontaneous synaptic activity was monitored using a high Cl^- concentration in the pipette that would result in a reversal potential for Cl− of about 0 mV (Groisman et al., 2020; Laplagne et al., 2007). Recordings from 6-week-old GFP^+ GCs at a negative membrane potential (−70 mV) showed spontaneous inhibitory postsynaptic currents (sIPSCs) with high frequency and fast rise time, corresponding to perisomatic inhibition (Fig. 3A-F). GCs expressing GFP at 6 wpi showed similar sIPSC frequency as unlabeled mature GCs, consistent with the notion that perisomatic functional connectivity does not change beyond this point. Interestingly, NL2 knockdown resulted in reduced frequency and amplitude, and slower rise time of perisomatic sIPSCs (Fig. 3B-F). To determine whether NL2 knockdown produces a broad alteration of GABAergic transmission beyond the perisomatic compartment, the holding potential ($V_{HOLDING}$) was then switched to 0 mV to enhance the driving force for distal dendritic responses, while minimizing proximal inputs. Spontaneous IPSCs in control GCs (both unlabeled GCs and 6 wpi GFP-GCs) displayed lower frequency and slower kinetics than perisomatic events, compatible with distal dendritic GABAergic inputs (Fig. 3G-L). Neurons expressing shNL2 displayed sIPSCs with similar amplitude, kinetics and frequency as those observed in control GCs, demonstrating that dendritic GABAergic inhibition was not modified by NL2 knockdown.

Two compatible scenarios may explain the decreased frequency of perisomatic events; one would be the reduced number of synaptic contacts suggested by the smaller synaptic areas shown by confocal analysis, and the second might be a diminished probability of neurotransmitter release (P_r) at presynaptic terminals (Bekkers & Stevens, 1990; Korn & Faber, 1991; Malinow & Tsien, 1990). On the other hand, the reduced amplitude and slow kinetics are likely consequence of postsynaptic alterations in the density and/or subunit composition of $GABA_A$ receptors (Lodge et al., 2021; Poulopoulos et al., 2009).

To gain further insight on the nature of synaptic changes induced by NL2 knockdown, we monitored postsynaptic responses evoked by direct stimulation of PV-INs. RV-shNL2-GFP or RV-SCR-GFP were delivered to the dentate gyrus of adult PV^{Cre};$CAG^{floxStopChR2}$ mice. Stimulation of PV-INs with blue laser pulses evoked inhibitory postsynaptic currents (eIPSCs) in 6-week-old GCs (Fig 4A,B)(Groisman et al., 2020). GCs expressing SCR or mature unlabeled neurons from the outer third of the GCL displayed synaptic responses with fast kinetics, typical of perisomatic GABAergic transmission (Groisman et al., 2020).

In contrast, responses from shNL2-GCs were slow, with a conspicuous lengthening of the decay phase (Fig. 4B-D).

Decreased NL2 expression might alter transmission at the pre- and/or postsynaptic sites. Quantal analysis was used to obtain additional hints on the nature of the observed changes (Korn & Faber, 1991). An indirect measurement derived from this analysis corresponds to the square of the coefficient of variation (CV^2), which depends on presynaptic variables such as the number of functional release sites and the release probability (Kraushaar & Jonas, 2000; Malinow & Tsien, 1990). While eIPSC amplitude showed only a slight decrease in GCs expressing shNL2, CV^2 was heightened, which is compatible with lower release probability or with a reduction in the number of release sites (Fig. 4E,F). Interestingly, eIPSCs with larger amplitude correlated with lower CV^2, suggesting that synaptic strength is mainly influenced by presynaptic parameters rather than postsynaptic receptor properties (Fig. 4G).

We next applied brief stimulation trains (5 pulses, 20 Hz) to analyze short-term plasticity in the PV-IN to GC synapse. In our recording conditions, eIPSC trains displayed short-term depression in GCs expressing both SCR and shNL2 (Fig. 4H-K). In particular, paired-pulse ratio in the second event of the train was higher in shNL2-GCs than in SCR-GCs, which is consistent with presynaptic modifications generated by the postsynaptic knockdown of NL2 (Fig 4K). Slow train responses in shNL2-expressing neurons were similar to those found in immature synapses of PV-INs contacting adult-born immature GCs (Fig. 4J)(Groisman et al., 2020).

To corroborate that NL2 signaling is restricted to proximal synapses, we stimulated GABAergic axons of the outer molecular layer using a monopolar electrode and measured distal dendritic responses. Evoked IPSCs were measured in 6 wpi GCs expressing SCR, shNL2 or in unlabeled mature GCs. Responses were mediated by $GABA_A$ receptors and blocked by picrotoxin (PTX, Fig. 5A,B). Evoked IPSCs displayed similar amplitude, rise and decay times for SCR, shNL2 and unlabeled GCs (Fig. 5C-E). These results demonstrate that NL2 is not relevant for distal dendritic inhibition in adult-born GCs, but it is crucial for the establishment and maturation of fast GABAergic transmission mediated by PV-INs.

4 DISCUSSION

In immature GCs, GABAergic transmission conveys slow depolarizing signals that are crucial for shaping their development and integration (Alvarez et al., 2016; Chancey et al., 2013; Doischer et al., 2008; Ge et al., 2006; Heigele et al., 2016; Lodge et al., 2021; Song et al., 2013). As GCs progress towards maturation, GABAergic inputs at multiple subcellular locations play distinctive roles to control input weights, firing rate and rhythms of activity (Hainmueller & Bartos, 2020). In particular, axonal projections of PV-INs coat the entire GCL and convey fast inhibition to limit the activation of all neurons in the layer, keeping overall dentate activity sparse. Newborn GCs develop under conditions of high excitation because they remain poorly connected to PV-IN axons until a late point in their development. In fact, the time at which fast PV-IN transmission is finally assembled is coincident with ending the period of enhanced excitability and plasticity of new GCs,

switching to the high activation threshold characteristic of mature GCs (Trinchero et al., 2021). Because new GCs grow through a compact layer of cell bodies and PV-IN axons, the delayed maturation of perisomatic inhibition is likely to respond to intrinsic mechanisms acting postsynaptically within the developing cell, which in turn may act retrogradely at the presynaptic terminal. Contacts between PV-INs and new GCs are formed early, but postsynaptic responses exhibit weak transmission with slow kinetics for several weeks until becoming progressively stronger and faster (Groisman et al., 2020; Remmers et al., 2020; Song et al., 2013; Vaden et al., 2020). There are different alternatives that could give rise to the remarkably slow synaptogenesis. One possibility would be that PV-IN terminals make early contacts that grow slowly in number and evolve in their postsynaptic subunit composition until reaching a final mature transmission after several weeks (Doischer et al., 2008; Lodge et al., 2021). An alternative view proposed that early transmission with immature characteristics arises by spillover from mature neighbor synapses rather than from physical contacts between PV-INs and developing GCs, which would occur later in development (Vaden et al., 2020). Our results show that appositions between PV-INs axons and adult-born GC cell bodies can be observed as early as 2 wpi supporting the idea of direct innervation, although it is possible that a spillover component contributes to postsynaptic responses in the more immature GCs targeted in POMC-EGFP mice (Vaden et al., 2020). We found that the area of apposition expanded substantially until 4 weeks, which would be consistent with an increase in the number of synaptic contacts. It is surprising that no further synaptic growth occurred between 4 and 8 weeks, the time window at which critical changes in strength and kinetics occur, crystalizing the final conversion to fast synaptic transmission (Groisman et al., 2020). These results are compatible with a view in which the number of perisomatic contacts by PV-INs grows until the 4^{th} week, and further changes in synaptic transmission arise from modifications in the pre- and/or postsynaptic machinery.

Although the temporal progression of adult-born GCs coupling to the inhibitory network has been largely addressed, little is known about the molecular mechanisms involved in their establishment and maturation, particularly in regard to perisomatic inhibition. In our view, a possible delayed expression of scaffolding proteins such as NL2 might explain the protracted maturation of the PV-IN synapse due to its well-known role in the specification of GABAergic perisomatic synapses (Panzanelli, Fruh, & Fritschy, 2017; Poulopoulos et al., 2009). To study the effects of NL2 loss-of-function in adult neurogenesis, we downregulated NL2 using a retrovirus expressing a specific shRNA delivered into new GCs and examined the outcome in synaptic morphology and function. In these experiments, NL2 knockdown occurred from the onset of GC development due to the early expression of retroviral constructs expressing shNL2 in proliferating progenitor cells, allowing us to assess chronic effects of NL2 manipulation in adult-born GCs at mature stages (6 to 8 wpi). Interestingly, the observed structural and functional effects are compatible with a scenario of protracted development of synapses lacking NL2: 1) reduced density of perisomatic PV-IN appositions and VGAT-positive puncta; 2) low frequency of sIPSCs; 3) small sIPSC amplitude; 4) slow kinetics of both spontaneous and evoked responses; 5) increased CV^2 and paired-pulse ratio of eIPSCs consistent with low P_r. Altogether, these features resemble immature synapses formed by PV-INs onto target cells reported in the developing and adult hippocampus (Doischer et al., 2008; Groisman et al., 2020; Hollrigel & Soltesz, 1997; Lodge et al., 2021;

Overstreet Wadiche, Bromberg, Bensen, & Westbrook, 2005; Sauer, Struber, & Bartos, 2012).

In terms of morphology, NL2 knockdown induced a significant reduction in the size of PV-IN appositions that was paralleled by a decline in VGAT immunoreactivity. These results suggested a decrease in the number of synaptic sites, which might also be accompanied by altered synaptic function. In fact, multiple changes were observed in synaptic transmission onto GCs expressing shNL2. Proximal spontaneous responses showed reduced frequency and amplitude, as well as slow rise time compared to controls. IPSCs evoked by direct optogenetic stimulation of PV-INs also displayed abnormal characteristics consisting in slower rise and decay time, as well as a reduced release probability that was inferred from short-term plasticity in response to pulse trains. The slow kinetics and small amplitude of synaptic responses in shNL2-expressing GCs might be consequence of altered receptor composition and density at the postsynaptic site. Accordingly, manipulation of NL2 expression was shown to affect multiple components of GABAergic synapses. A consistent finding across several brain regions is that reduced or abolished NL2 expression decreases the density of $GABA_A$ receptors and the scaffolding protein gephyrin, while presynaptic components seemed to remain unaltered (Babaev et al., 2016; Gibson, Huber, & Sudhof, 2009; Jedlicka et al., 2011; Panzanelli et al., 2017; Poulopoulos et al., 2009). Yet, the reduction in synaptic number and P_r found in adult-born GCs expressing shNL2 seem to point to retrograde signaling whereby presynaptic terminals exhibit impaired synaptic formation or function. Those terminals arise from the same PV-INs that are capable of fast perisomatic transmission onto neighbor mature GCs bearing normal levels of NL2. Interestingly, mechanisms of plasticity expressed as presynaptic modifications imposed by target neurons have been observed in several central circuits (Reyes et al., 1998; Scanziani, Gahwiler, & Charpak, 1998; Schinder, Berninger, & Poo, 2000).

The specificity of NL2 requirement for perisomatic synapses was validated by the lack of effect of NL2 knockdown in spontaneous responses from distal compartments and also in recordings evoked by electrical stimulation of GABAergic axons in the outer molecular layer. This is in agreement and with previous observations that NL2 is critical for synapse formation and maintenance, and also that PV-IN and SST-IN synapses are regulated by distinct molecular mechanisms (Babaev et al., 2016; Gibson et al., 2009; Hoon et al., 2009; Horn & Nicoll, 2018; Kahle et al., 2013; Liang et al., 2015; Poulopoulos et al., 2009). In light of our results, we propose that expression of NL2 might be instrumental for ending the developmental period of high excitability in immature GCs and promote the transition towards sparse levels of activity characteristic of mature GCs. This function would be critical for preserving the delicate balance between excitation and inhibition that is required to maintain overall stability during circuit remodeling by neurogenesis.

ACKNOWLEDGMENTS

We thank Mariela Trinchero for critical comments on the manuscript, and the members of the A.F.S. and Emilio Kropff labs for insightful discussions. A.F.S. and D.P.G. are investigators in the Consejo Nacional de Investigaciones Científicas y Técnicas (CONICET). A.I.G. was supported by a CONICET fellowship. A.A.A was supported by a fellowship from the Secretary of Education, Science, Technology and Innovation (SECTEI) of Mexico City. This work was supported by grants from the Argentine Agency for the Promotion of Science and

Technology to D.G. (PICT 2017-0389) and A.F.S. (PICT2016-0675), and the National Institute Of Neurological Disorders And Stroke (NINDS) and Fogarty International Center (FIC) (R01NS103758) to A.F.S.

DATA AVAILABILITY

The data that support the findings of this study are available from the corresponding author upon reasonable request.

REFERENCES

Ali H, Marth L, & Krueger-Burg D (2020). Neuroligin-2 as a central organizer of inhibitory synapses in health and disease. Sci Signal, 13(663). doi:10.1126/scisignal.abd8379

Alvarez DD, Giacomini D, Yang SM, Trinchero MF, Temprana SG, Buttner KA, … Schinder AF (2016). A disynaptic feedback network activated by experience promotes the integration of new granule cells. Science, 354(6311), 459–465. doi:10.1126/science.aaf2156 [PubMed: 27789840]

Babaev O, Botta P, Meyer E, Muller C, Ehrenreich H, Brose N, … Krueger-Burg D (2016). Neuroligin 2 deletion alters inhibitory synapse function and anxiety-associated neuronal activation in the amygdala. Neuropharmacology, 100, 56–65. doi:10.1016/j.neuropharm.2015.06.016 [PubMed: 26142252]

Bekkers JM, & Stevens CF (1990). Presynaptic mechanism for long-term potentiation in the hippocampus. Nature, 346(6286), 724–729. doi:10.1038/346724a0 [PubMed: 2167454]

Chancey JH, Adlaf EW, Sapp MC, Pugh PC, Wadiche JI, & Overstreet-Wadiche LS (2013). GABA depolarization is required for experience-dependent synapse unsilencing in adult-born neurons. J Neurosci, 33(15), 6614–6622. doi:10.1523/JNEUROSCI.0781-13.2013 [PubMed: 23575858]

Chanda S, Hale WD, Zhang B, Wernig M, & Sudhof TC (2017). Unique versus Redundant Functions of Neuroligin Genes in Shaping Excitatory and Inhibitory Synapse Properties. J Neurosci, 37(29), 6816–6836. doi:10.1523/JNEUROSCI.0125-17.2017 [PubMed: 28607166]

Chaudhry FA, Reimer RJ, Bellocchio EE, Danbolt NC, Osen KK, Edwards RH, & Storm-Mathisen J (1998). The vesicular GABA transporter, VGAT, localizes to synaptic vesicles in sets of glycinergic as well as GABAergic neurons. J Neurosci, 18(23), 9733–9750. [PubMed: 9822734]

Chih B, Engelman H, & Scheiffele P (2005). Control of excitatory and inhibitory synapse formation by neuroligins. Science, 307(5713), 1324–1328. [PubMed: 15681343]

Chubykin AA, Atasoy D, Etherton MR, Brose N, Kavalali ET, Gibson JR, & Sudhof TC (2007). Activity-dependent validation of excitatory versus inhibitory synapses by neuroligin-1 versus neuroligin-2. Neuron, 54(6), 919–931. doi:10.1016/j.neuron.2007.05.029 [PubMed: 17582332]

Crosby KC, Gookin SE, Garcia JD, Hahm KM, Dell'Acqua ML, & Smith KR (2019). Nanoscale Subsynaptic Domains Underlie the Organization of the Inhibitory Synapse. Cell Rep, 26(12), 3284–3297 e3283. doi:10.1016/j.celrep.2019.02.070 [PubMed: 30893601]

Dieni CV, Panichi R, Aimone JB, Kuo CT, Wadiche JI, & Overstreet-Wadiche L (2016). Low excitatory innervation balances high intrinsic excitability of immature dentate neurons. Nat Commun, 7, 11313. doi:10.1038/ncomms11313 [PubMed: 27095423]

Doischer D, Hosp JA, Yanagawa Y, Obata K, Jonas P, Vida I, & Bartos M (2008). Postnatal differentiation of basket cells from slow to fast signaling devices. J Neurosci, 28(48), 12956–12968. doi:10.1523/JNEUROSCI.2890-08.2008 [PubMed: 19036989]

Fritschy JM, & Panzanelli P (2014). GABAA receptors and plasticity of inhibitory neurotransmission in the central nervous system. Eur J Neurosci, 39(11), 1845–1865. doi:10.1111/ejn.12534 [PubMed: 24628861]

Ge S, Goh EL, Sailor KA, Kitabatake Y, Ming GL, & Song H (2006). GABA regulates synaptic integration of newly generated neurons in the adult brain. Nature, 439(7076), 589–593. doi:10.1038/nature04404 [PubMed: 16341203]

Ge S, Yang CH, Hsu KS, Ming GL, & Song H (2007). A critical period for enhanced synaptic plasticity in newly generated neurons of the adult brain. Neuron, 54(4), 559–566. doi:10.1016/j.neuron.2007.05.002 [PubMed: 17521569]

Gibson JR, Huber KM, & Sudhof TC (2009). Neuroligin-2 deletion selectively decreases inhibitory synaptic transmission originating from fast-spiking but not from somatostatin-positive interneurons. J Neurosci, 29(44), 13883–13897. doi:10.1523/JNEUROSCI.2457-09.2009 [PubMed: 19889999]

Goncalves JT, Schafer ST, & Gage FH (2016). Adult Neurogenesis in the Hippocampus: From Stem Cells to Behavior. Cell, 167(4), 897–914. doi:10.1016/j.cell.2016.10.021 [PubMed: 27814520]

Groisman AI, Yang SM, & Schinder AF (2020). Differential Coupling of Adult-Born Granule Cells to Parvalbumin and Somatostatin Interneurons. Cell Rep, 30(1), 202–214 e204. doi:10.1016/j.celrep.2019.12.005 [PubMed: 31914387]

Hainmueller T, & Bartos M (2020). Dentate gyrus circuits for encoding, retrieval and discrimination of episodic memories. Nat Rev Neurosci, 21(3), 153–168. doi:10.1038/s41583-019-0260-z [PubMed: 32042144]

Heigele S, Sultan S, Toni N, & Bischofberger J (2016). Bidirectional GABAergic control of action potential firing in newborn hippocampal granule cells. Nat Neurosci, 19(2), 263–270. doi:10.1038/nn.4218 [PubMed: 26752162]

Hollrigel GS, & Soltesz I (1997). Slow kinetics of miniature IPSCs during early postnatal development in granule cells of the dentate gyrus. J.Neurosci, 17(13), 5119–5128. [PubMed: 9185549]

Hoon M, Bauer G, Fritschy JM, Moser T, Falkenburger BH, & Varoqueaux F (2009). Neuroligin 2 controls the maturation of GABAergic synapses and information processing in the retina. J Neurosci, 29(25), 8039–8050. doi:10.1523/JNEUROSCI.0534-09.2009 [PubMed: 19553444]

Horn ME, & Nicoll RA (2018). Somatostatin and parvalbumin inhibitory synapses onto hippocampal pyramidal neurons are regulated by distinct mechanisms. Proc Natl Acad Sci U S A, 115(3), 589–594. doi:10.1073/pnas.1719523115 [PubMed: 29295931]

Hosp JA, Struber M, Yanagawa Y, Obata K, Vida I, Jonas P, & Bartos M (2014). Morpho-physiological criteria divide dentate gyrus interneurons into classes. Hippocampus, 24(2), 189–203. doi:10.1002/hipo.22214 [PubMed: 24108530]

Huang ZJ, & Scheiffele P (2008). GABA and neuroligin signaling: linking synaptic activity and adhesion in inhibitory synapse development. Curr Opin Neurobiol, 18(1), 77–83. doi:10.1016/j.conb.2008.05.008 [PubMed: 18513949]

Jedlicka P, Hoon M, Papadopoulos T, Vlachos A, Winkels R, Poulopoulos A, … Schwarzacher SW (2011). Increased dentate gyrus excitability in neuroligin-2-deficient mice in vivo. Cereb Cortex, 21(2), 357–367. doi:10.1093/cercor/bhq100 [PubMed: 20530218]

Kahle KT, Deeb TZ, Puskarjov M, Silayeva L, Liang B, Kaila K, & Moss SJ (2013). Modulation of neuronal activity by phosphorylation of the K-Cl cotransporter KCC2. Trends Neurosci, 36(12), 726–737. doi:10.1016/j.tins.2013.08.006 [PubMed: 24139641]

Kepecs A, & Fishell G (2014). Interneuron cell types are fit to function. Nature, 505(7483), 318–326. doi:10.1038/nature12983 [PubMed: 24429630]

Korn H, & Faber DS (1991). Quantal analysis and synaptic efficacy in the CNS. Trends Neurosci., 14(10), 439–445. [PubMed: 1722362]

Kraushaar U, & Jonas P (2000). Efficacy and stability of quantal GABA release at a hippocampal interneuron-principal neuron synapse. J.Neurosci, 20(15), 5594–5607. [PubMed: 10908596]

Krzisch M, Fulling C, Jabinet L, Armida J, Gebara E, Casse F, … Toni N (2016). Synaptic Adhesion Molecules Regulate the Integration of New Granule Neurons in the Postnatal Mouse Hippocampus and their Impact on Spatial Memory. Cereb Cortex. doi:10.1093/cercor/bhw217

Laplagne DA, Espósito MS, Piatti VC, Morgenstern NA, Zhao C, van Praag H, … Schinder AF (2006). Functional convergence of neurons generated in the developing and adult hippocampus. PLoS.Biol, 4(12), e409. [PubMed: 17121455]

Laplagne DA, Kamienkowski JE, Espósito MS, Piatti VC, Zhao C, Gage FH, & Schinder AF (2007). Similar GABAergic inputs in dentate granule cells born during embryonic and adult neurogenesis. Eur.J.Neurosci, 25(10), 2973–2981. [PubMed: 17509085]

Liang J, Xu W, Hsu YT, Yee AX, Chen L, & Sudhof TC (2015). Conditional neuroligin-2 knockout in adult medial prefrontal cortex links chronic changes in synaptic inhibition to cognitive impairments. Mol Psychiatry, 20(7), 850–859. doi:10.1038/mp.2015.31 [PubMed: 25824299]

Lodge M, Hernandez MC, Schulz JM, & Bischofberger J (2021). Sparsification of AP firing in adult-born hippocampal granule cells via voltage-dependent alpha5-GABAA receptors. Cell Rep, 37(1), 109768. doi:10.1016/j.celrep.2021.109768 [PubMed: 34610304]

Malinow R, & Tsien RW (1990). Presynaptic enhancement shown by whole-cell recordings of long-term potentiation in hippocampal slices. Nature, 346(6280), 177–180. doi:10.1038/346177a0 [PubMed: 2164158]

Marin-Burgin A, Mongiat LA, Pardi MB, & Schinder AF (2012). Unique Processing During a Period of High Excitation/Inhibition Balance in Adult-Born Neurons. Science. doi:science.1214956 [pii]

Mongiat LA, & Schinder AF (2011). Adult neurogenesis and the plasticity of the dentate gyrus network. Eur J Neurosci, 33(6), 1055–1061. doi:10.1111/j.1460-9568.2011.07603.x [PubMed: 21395848]

Moreno-Jimenez EP, Flor-Garcia M, Terreros-Roncal J, Rabano A, Cafini F, Pallas-Bazarra N, … Llorens-Martin M (2019). Adult hippocampal neurogenesis is abundant in neurologically healthy subjects and drops sharply in patients with Alzheimer's disease. Nat Med, 25(4), 554–560. doi:10.1038/s41591-019-0375-9 [PubMed: 30911133]

Overstreet Wadiche LS, Bromberg DA, Bensen AL, & Westbrook GL (2005). GABAergic signaling to newborn neurons in dentate gyrus. J.Neurophysiol, 94 (6), 4528–4532. [PubMed: 16033936]

Panzanelli P, Fruh S, & Fritschy JM (2017). Differential role of GABAA receptors and neuroligin 2 for perisomatic GABAergic synapse formation in the hippocampus. Brain Struct Funct, 222(9), 4149–4161. doi:10.1007/s00429-017-1462-7 [PubMed: 28643105]

Paxinos G, & Franklin KBJ (2001). The mouse brain in stereotaxic coordinates. San Diego: Academic Press.

Poulopoulos A, Aramuni G, Meyer G, Soykan T, Hoon M, Papadopoulos T, … Varoqueaux F (2009). Neuroligin 2 drives postsynaptic assembly at perisomatic inhibitory synapses through gephyrin and collybistin. Neuron, 63(5), 628–642. doi:10.1016/j.neuron.2009.08.023 [PubMed: 19755106]

Remmers CL, Castillon CCM, Armstrong JN, & Contractor A (2020). Recruitment of parvalbumin and somatostatin interneuron inputs to adult born dentate granule neurons. Sci Rep, 10(1), 17522. doi:10.1038/s41598-020-74385-2 [PubMed: 33067500]

Reyes A, Lujan R, Rozov A, Burnashev N, Somogyi P, & Sakmann B (1998). Target-cell-specific facilitation and depression in neocortical circuits. Nat.Neurosci, 1(4), 279–285. [PubMed: 10195160]

Sauer JF, Struber M, & Bartos M (2012). Interneurons provide circuit-specific depolarization and hyperpolarization. J Neurosci, 32(12), 4224–4229. doi:10.1523/JNEUROSCI.5702-11.2012 [PubMed: 22442084]

Scanziani M, Gahwiler BH, & Charpak S (1998). Target cell-specific modulation of transmitter release at terminals from a single axon. Proc Natl Acad Sci U S A, 95(20), 12004–12009. doi:10.1073/pnas.95.20.12004 [PubMed: 9751780]

Schinder AF, Berninger B, & Poo M (2000). Postsynaptic target specificity of neurotrophin-induced presynaptic potentiation. Neuron, 25(1), 151–163. [PubMed: 10707980]

Song J, Sun J, Moss J, Wen Z, Sun GJ, Hsu D, … Song H (2013). Parvalbumin interneurons mediate neuronal circuitry-neurogenesis coupling in the adult hippocampus. Nat Neurosci, 16(12), 1728–1730. doi:10.1038/nn.3572 [PubMed: 24212671]

Song J, Zhong C, Bonaguidi MA, Sun GJ, Hsu D, Gu Y, … Song H (2012). Neuronal circuitry mechanism regulating adult quiescent neural stem-cell fate decision. Nature, 489(7414), 150–154. doi:10.1038/nature11306 [PubMed: 22842902]

Temprana SG, Mongiat LA, Yang SM, Trinchero MF, Alvarez DD, Kropff E, … Schinder AF (2015). Delayed coupling to feedback inhibition during a critical period for the integration of adult-born granule cells. Neuron, 85(1), 116–130. doi:10.1016/j.neuron.2014.11.023 [PubMed: 25533485]

Trinchero MF, Giacomini D, & Schinder AF (2021). Dynamic interplay between GABAergic networks and developing neurons in the adult hippocampus. Curr Opin Neurobiol, 69, 124–130. doi:10.1016/j.conb.2021.03.008 [PubMed: 33873060]

Vaden RJ, Gonzalez JC, Tsai MC, Niver AJ, Fusilier AR, Griffith CM, … Overstreet-Wadiche L (2020). Parvalbumin interneurons provide spillover to newborn and mature dentate granule cells. Elife, 9. doi:10.7554/eLife.54125

van Praag H, Schinder AF, Christie BR, Toni N, Palmer TD, & Gage FH (2002). Functional neurogenesis in the adult hippocampus. Nature, 415(6875), 1030–1034. doi:10.1038/4151030a [PubMed: 11875571]

Varoqueaux F, Aramuni G, Rawson RL, Mohrmann R, Missler M, Gottmann K, … Brose N (2006). Neuroligins determine synapse maturation and function. Neuron, 51(6), 741–754. doi:10.1016/j.neuron.2006.09.003 [PubMed: 16982420]

Yogev S, & Shen K (2014). Cellular and molecular mechanisms of synaptic specificity. Annu Rev Cell Dev Biol, 30, 417–437. doi:10.1146/annurev-cellbio-100913-012953 [PubMed: 25150010]

Yuan M, Meyer T, Benkowitz C, Savanthrapadian S, Ansel-Bollepalli L, Foggetti A, … Bartos M (2017). Somatostatin-positive interneurons in the dentate gyrus of mice provide local- and long-range septal synaptic inhibition. Elife, 6. doi:10.7554/eLife.21105

Zhang B, Chen LY, Liu X, Maxeiner S, Lee SJ, Gokce O, & Sudhof TC (2015). Neuroligins Sculpt Cerebellar Purkinje-Cell Circuits by Differential Control of Distinct Classes of Synapses. Neuron, 87(4), 781–796. doi:10.1016/j.neuron.2015.07.020 [PubMed: 26291161]

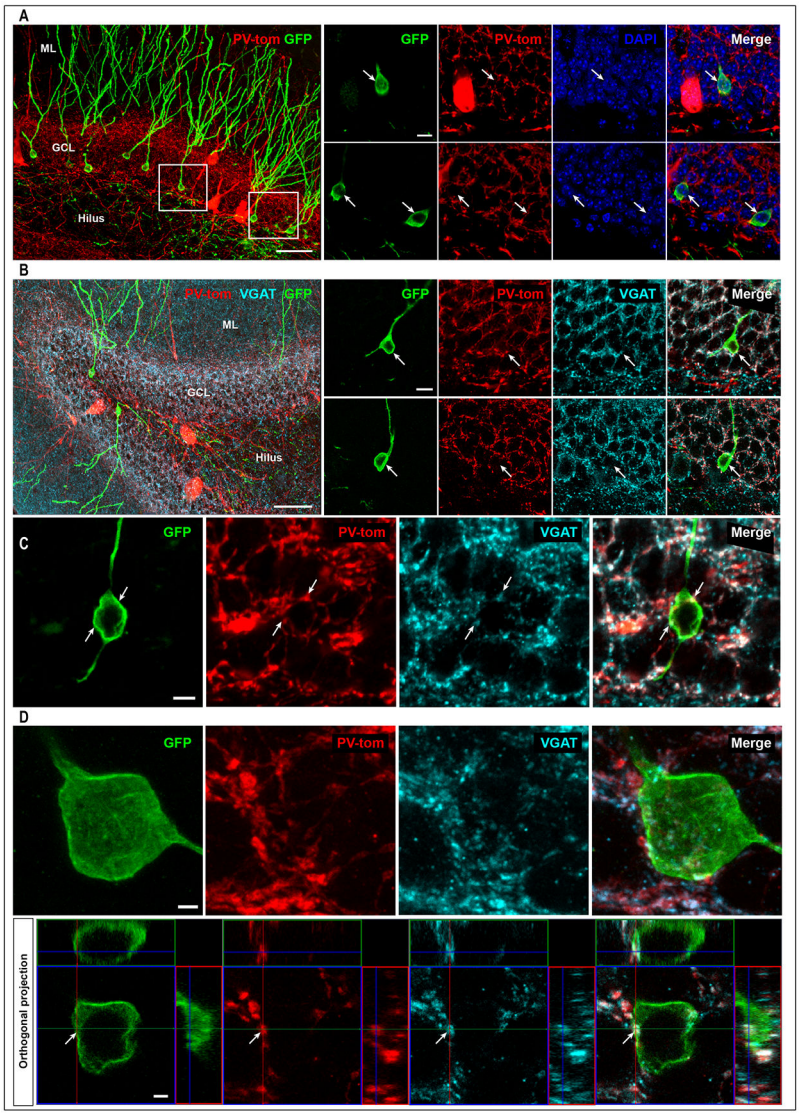

Figure 1. Perisomatic inhibition by PV-INs onto adult-born GCs revealed by confocal imaging.
Images display 8 wpi GCs labeled with RV-ChR2-GFP in PV^{Cre};$CAG^{floxStop\text{-}tdTomato}$ mice. **(A)** *Left panel*, Confocal projections of the dentate gyrus highlighting adult-born GCs (green) and PV-INs (red) intermingled within the GCL. Scale bar: 50 μm. *Right panels*, images displaying single optical sections of PV-IN terminals surrounding GC somas labeled with DAPI (cyan). Scale bar: 10 μm. **(B)** Image displaying PV-INs and VGAT immunofluorescence (cyan) in the GCL. Scale bar: 50 μm. *Right panels*, single confocal planes displaying VGAT and PV-IN terminals surrounding GC somas. Scale bar: 10 μm. **(C)** Images displaying single optical sections of PV-IN terminals colocalizing with VGAT (cyan) throughout the GCL. Note that both PV-INs and VGAT labels display colocalization sites around the GFP-labeled soma (arrows). Scale bar: 5 μm. **(D)** Three-dimensional reconstruction of an adult-born GC soma surrounded by PV-IN terminals colocalizing with VGAT (top panels). Orthogonal projections (bottom panels) reveal colocalization of PV-INs terminals, VGAT, and a GFP-labeled GC (arrow). Scale bars: 2 μm. ML: molecular layer.

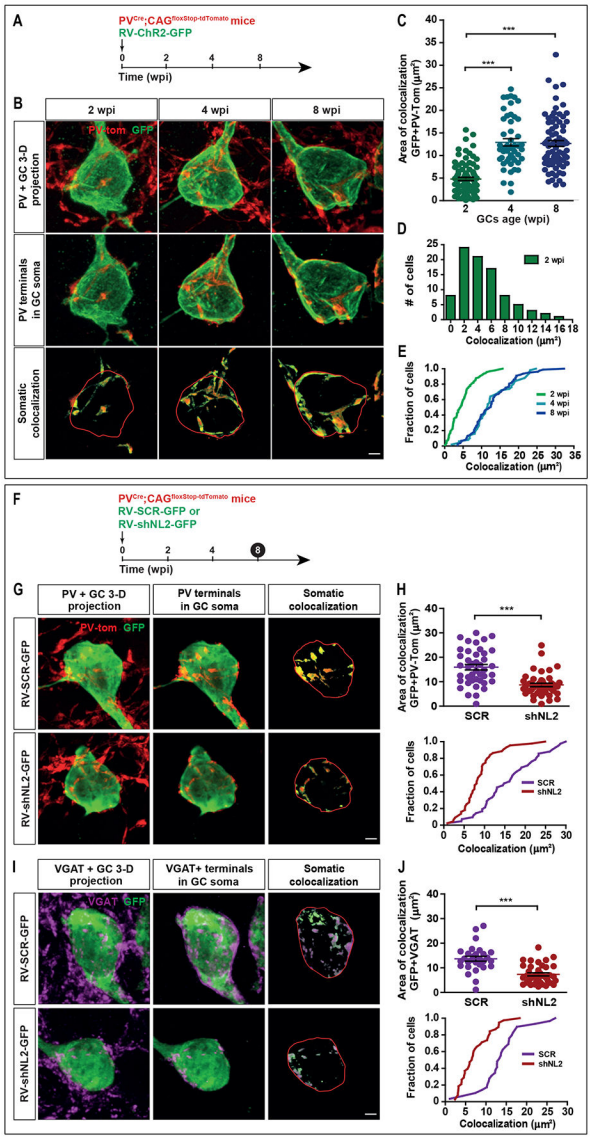

Figure 2. Perisomatic synaptogenesis in newborn GCs requires NL2.

(A) Experimental design. GCs expressing RV-ChR2-GFP in PV^{Cre};$CAG^{floxStoptdTomato}$ mice were analyzed at the indicated times post injection. **(B)** Representative 3-D reconstructions of individual adult-born GCs at 2, 4 and 8 wpi (green) surrounded by PV-IN projections (red). Middle panels show processed images depicting the appositions of PV-IN terminals onto the cell soma. Bottom panels show optimized projections after plane-by-plane detection of PV-IN and GC colocalization. Scale bar: 2µm. **(C)** Projected area of colocalization between GC somas and PV-IN terminals at different ages. Dots represent individual neurons. (***) denote $p < 0.001$ after Kruskal-Wallis' test followed by Dunn's post hoc. **(D)** Distribution of overlap areas between PV-Tom and GFP for 2 wpi GCs. **(E)** Cumulative distributions corresponding to values displayed in (C). **(F)** Experimental design. New GCs labeled with RV-SCR-GFP or RV-shNL2-GFP in PV^{Cre};$CAG^{floxStoptdTomato}$ mice were studied at 8 wpi. **(G)** Representative 3-D reconstructions of individual GCs expressing SCR-GFP (top panels) or shNL2-GFP (bottom panels) surrounded by PV-IN

projections (red). Middle columns show processed images depicting the appositions of PV-IN terminals onto the cell soma. Right columns show optimized projections after plane-by-plane detection of PV-IN and GC colocalization. Scale bar: 2 μm. **(H)** *Top panel*: Projected area of colocalization between GC somas and PV-IN terminals for SCR and shNL2. (***) denote statistical comparisons done using Mann-Whitney's test with $p < 0.001$. *Bottom panel:* cumulative distribution of colocalization area in SCR and shNL2 cells. **(I)** Three-dimensional reconstructions of individual GCs expressing SCR-GFP or shNL2-GFP surrounded by VGAT immunofluorescence (cyan). Scale bar: 2 μm. **(J)** Area of somatic apposition of VGAT terminals (*top panels*) and cumulative distribution (*bottom panel*). (***) denote $p < 0.001$ after Mann-Whitney's test. Sample sizes are N = 85 for 2 wpi GFP-GCs (4 mice), N = 45 for 4 wpi GFP-GCs (4 mice), N = 29 - 80 for 8 wpi GFP-GCs (4 mice), N = 29 - 72 for SCR-GCs (8 mice), and N = 38 - 82 for shNL2-GCs (8 mice). Horizontal bars denote mean ± SEM.

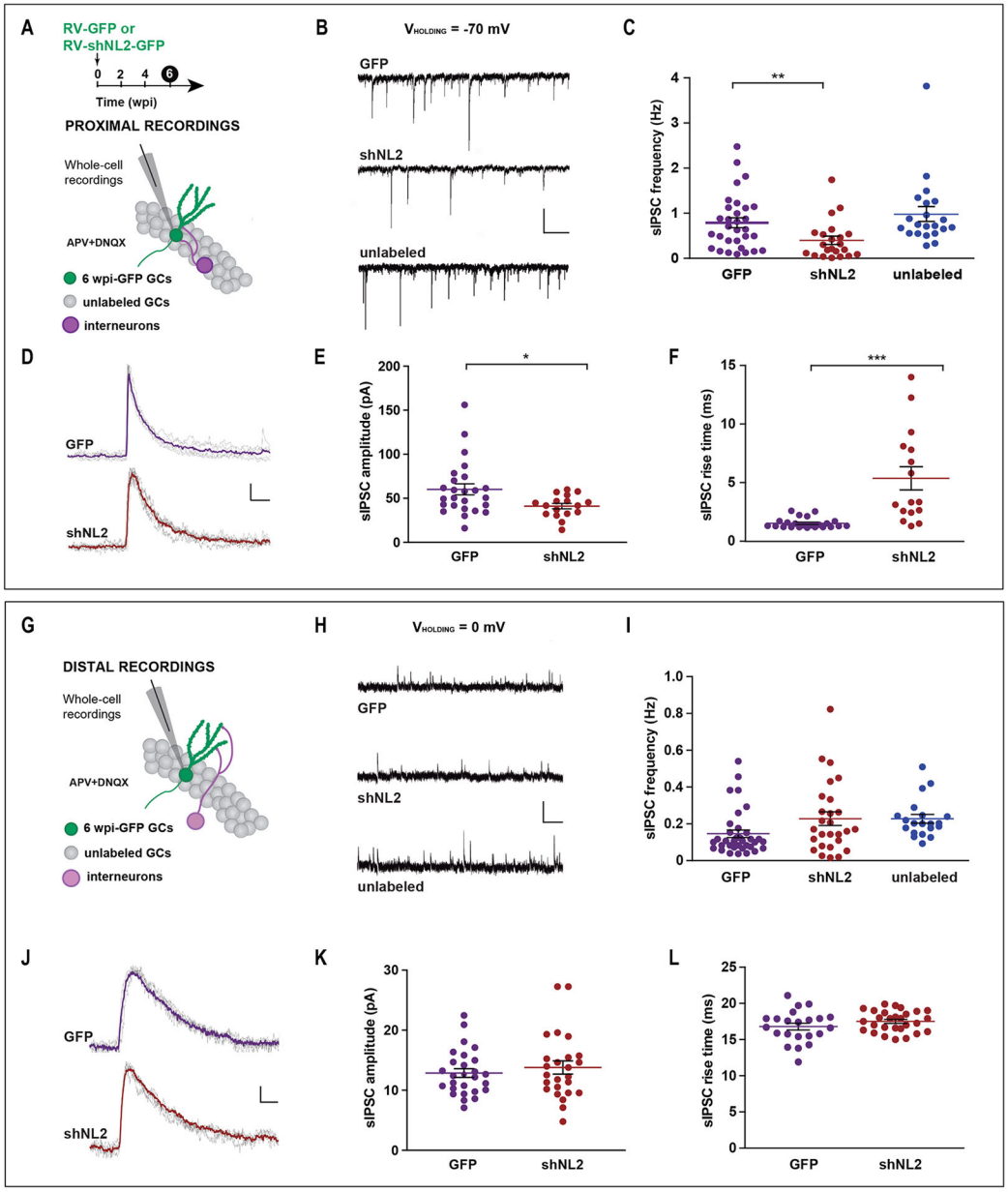

Figure 3. NL2 knockdown impairs spontaneous GABAergic transmission at proximal synapses.

(A) Experimental scheme. Adult-born GCs were labeled using RV-GFP or RV-shNL2-GFP. Whole-cell recordings were carried out at 6 wpi in the presence of APV (100 μM) and DNQX (20 μM) at $V_{HOLDING}$ = −70 mV, to detect proximal sIPSCs. **(B)** Representative sIPSC recordings performed in GCs expressing GFP, shNL2-GFP or unlabeled (outer third of the GCL). Scale bars: 100 pA, 5 s. **(C)** sIPSC frequency. Dots correspond to individual neurons. **(D)** Examples of normalized sIPSCs to highlight differences in kinetics. Traces depict normalized individual sweeps (gray) and their average (colored) corresponding to single neurons. Scale bars: 0.2 a.u., 25 ms. **(E, F)** sIPSC amplitude and rise time. Dots correspond to individual neurons. **(G)** Experimental scheme for distal sIPSC recordings at $V_{HOLDING}$ = 0 mV. **(H)** Representative sIPSC recordings performed in GCs expressing

GFP, shNL2-GFP or unlabeled (outer third of the GCL). Scale bars: 20 pA, 5 s. **(I)** sIPSC frequency. **(J)** Examples of normalized sIPSCs corresponding to individual neurons. Scale bars: 0.2 a.u, 100 ms. **(K, L)** sIPSC amplitude and rise time. Sample sizes are N = 23 GFP GCs (7 mice), N = 16 shNL2 GCs (7 mice), and N = 21 unlabeled GCs (10 mice). Bars denote mean ± SEM. (*), (**) and (***) denote $p < 0.05$, $p < 0.01$ and $p < 0.001$ after Mann-Whitney's test.

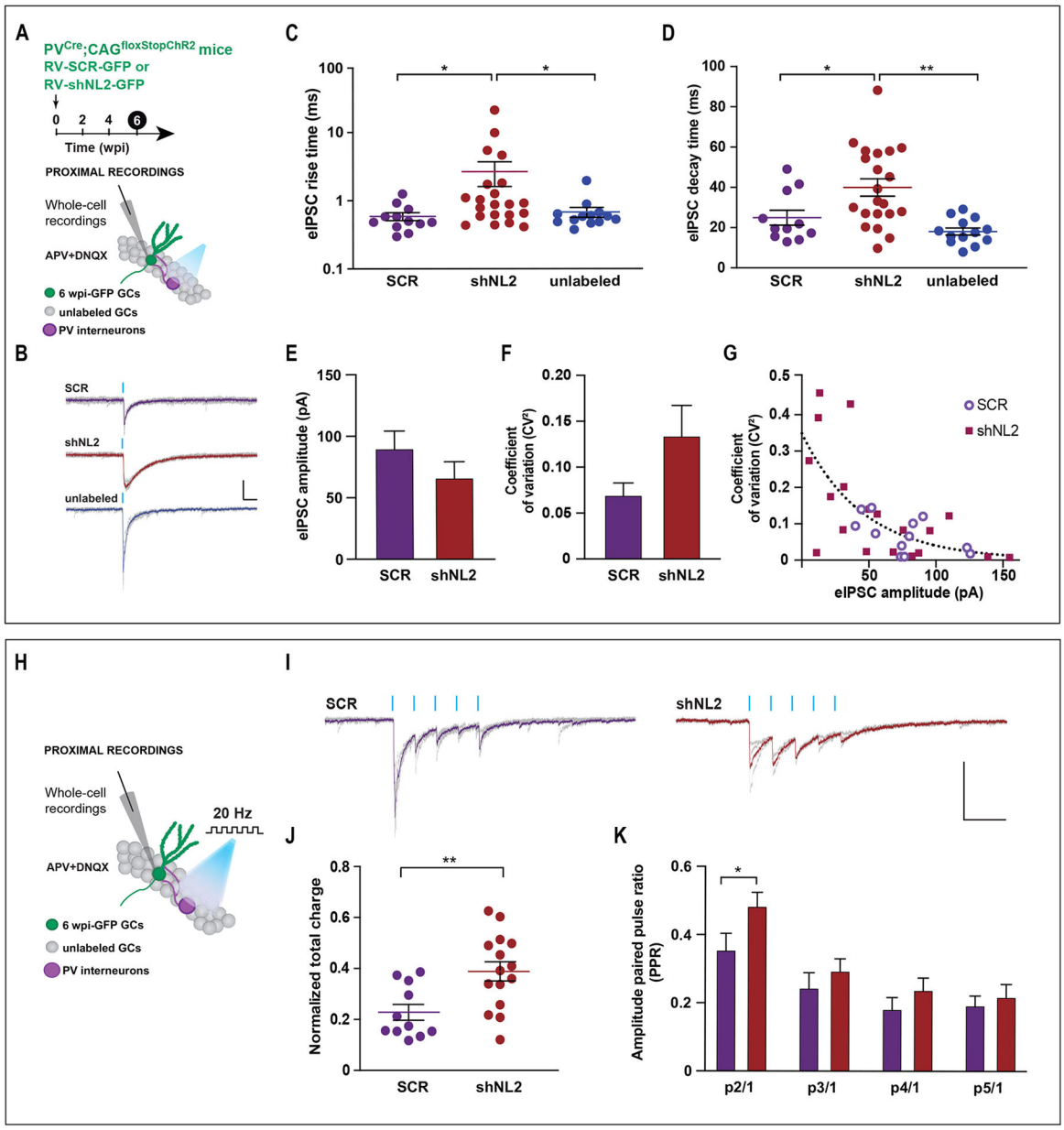

Figure 4. Altered presynaptic properties of perisomatic contacts onto new GCs with reduced NL2 expression revealed by evoked transmission.

(A) Experimental scheme. $PV^{Cre};CAG^{floxStopChR2}$ mice received RV-SCR-GFP or RV-shNL2-GFP to label adult-born GCs. Responses (eIPSCs) were evoked by single laser pulses (0.2 ms, blue marks) delivered at 0.07 Hz in the presence of APV (100 μM) and DNQX (20 μM). Whole-cell recordings were carried out in 6 wpi GCs at $V_{HOLDING}$= −70 mV. **(B)** Representative recordings in new GC expressing SCR-GFP, shNL2-GFP, or unlabeled (outer third of the GCL). Traces depict individual sweeps (gray) and their average (colored). Scale bars: 50 pA, 50 ms. **(C, D)** eIPSCs rise and decay time. Dots correspond to individual neurons. **(E)** Proximal eIPSCs peak amplitude. **(F)** Coefficient of variation $CV^2 = (\sigma/m)^2$; σ and m are the standard deviation and mean eIPSC amplitude for each cell. **(G)** CV^2 vs eIPSC amplitude for shNL2 and SCR, suggesting higher Pr for the larger events.

A significant Spearman correlation ($p < 0.001$) between CV2 and the eIPSC amplitude was obtained for both datasets together (shNL2 + SCR). The global dataset was fitted to a single exponential decay ($y = y_0 . e^{-\frac{x}{\tau}}$, with $y_0 = 0.35$, $\tau = 45.7$ pA), denoted by a dotted line. **(H)** Experimental scheme for responses evoked by pulse trains (5 pulses at 20 Hz) delivered at 0.03 Hz. **(I)** Representative recordings obtained from GCs expressing SCR- GFP or shNL2-GFP. Scale bars: 100 pA, 100 ms. **(J)** Normalized charge for eIPSCs in response to the entire train. **(K)** Individual paired pulse ratio (PPR) measured as the peak amplitude of each pulse response and normalized to the first pulse of each train. Sample sizes are N = 12 for SCR (7 mice), N = 15 for shNL2 (9 mice) and N = 13 unlabeled (9 mice). Bars denote mean ± SEM. (*) and (**) denote $p < 0.05$ and $p < 0.01$ after Mann-Whitney's test.

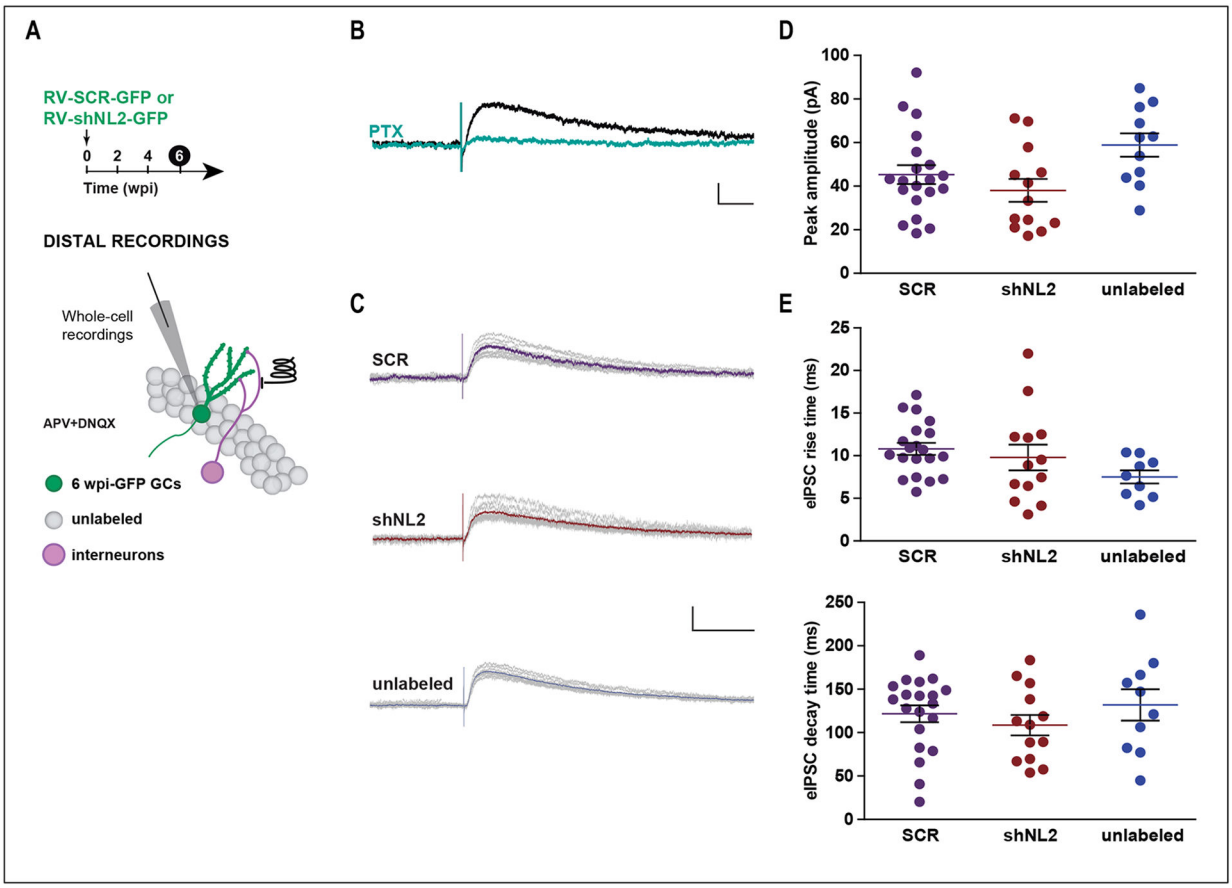

Figure 5. Unaltered GABAergic transmission at distal dendrites in new GCs with NL2 knockdown.

(A) Experimental scheme. Adult-born GCs were labeled using RV-GFP, RV-SCR-GFP or RV-shNL2-GFP. Distal dendritic responses (eIPSCs) were evoked by electrical stimulation of the outer molecular layer (0.2 ms) at 0.07 Hz in the presence of APV (100 μM) and DNQX (20 μM). Whole-cell recordings were carried out in 6 wpi GCs at $V_{HOLDING}$ = −30 mV. **(B)** Example traces show responses blocked by PTX (100 μM) in a 6 wpi GC expressing SCR-GFP. Scale bars: 25 pA, 50 ms. **(C)** Representative recordings in new GC expressing SCR-GFP, shNL2-GFP, or unlabeled (outer third of the GCL). Traces depict normalized sweeps (gray) and their average (colored). Scale bars: 50 pA, 50 ms. **(D)** Distal eIPSC peak amplitude, rise and decay times. Dots correspond to individual neurons. Sample sizes are N = 20 for SCR (6 mice), N = 13 for shNL2 (7 mice) and N = 9 unlabeled (6 mice). Bars denote mean ± SEM. Statistical comparisons revealed no differences among the groups.

Table 1.

Morphological parameters and intrinsic properties of adult-born GCs under NL2 knockdown

	Age (wpi)					
	2	4	≥ 6			Mature
RV-labeling	**GFP/ChR2**	**GFP/ChR2**	**GFP/ChR2**	**SCR**	**shNL2**	**Unlabeled**
Soma size (μm²)	87.0 ± 1 .8 [a] N = 85	92.0 ± 1.7 [b] N = 45	78.0 ± 2.2 [a,b] N = 80	93.0 ± 1.5 [c] N = 72	77.0 ± 1.4 [c] N = 82	-
PV-GFP colocalization (μm²)	4.8 ± 0.3 [d,e] N = 85	12.9 ± 0.8 [d] N = 45	12.8 ± 0.6 [e] N = 80	15.9 ± 1.1 [f] N = 43	8.9 ± 0.7 [f] N = 44	-
PV-GFP colocalization (% soma area)	5.8 ± 0.4 [g,h] N = 85	13.8 ± 0.9 [g] N = 45	15.7 ± 0.7 [h] N = 80	17 ± 1.1 [i] N = 43	11.8 ± 1.0 [i] N = 44	-
VGAT-GFP colocalization (μm²)	-	-	15.5 ± 1.1 [j] N = 29	13.7 ± 1.0 [k] N = 29	7.3 ± 0.6 [j,k] N = 38	-
VGAT-GFP colocalization (% soma area)	-	-	19.6 ± 1.3 [l] N = 29	16.1 ± 0.8 [m] N = 29	9.0 ± 0.7 [l,m] N = 38	-
Dendritic length (μm)	241 ± 14 [n,o] N = 40	455 ± 31 [n] N = 24	525 ± 30 [o] N = 35	-	486 ± 30 N = 33	-
$V_{resting}$(mV)			−76.0 ± 1.5 N= 10	−74.0 ± 0.5 N = 16	−74.5 ± 1.4 N = 20	−75.0 ± 1.0 N = 15
R_{input}(MΩ)			295 ± 20 [p] N = 26	259 ± 22 [q] N = 16	422 ± 35 [p,q] N = 43	292 ± 22 N = 15
C_m(pF)			56 ± 3 N = 26	50 ± 4 N = 16	45 ± 4 N = 27	48 ± 3 N = 16

Mean ± SEM values are shown, with N representing the number of cells. $V_{resting}$, resting potential; C_m, membrane capacitance; R_{input}, input resistance. The dendritic length was quantified in adult-born GCs expressing RV-ShNL2 at 2 and 4 wpi with no significant effect when compared to RV-GFP.

Statistical comparisons are represented with superindexes:

([a]) and ([b]) denote $p < 0.01$ and $p < 0.001$ after Kruskal Wallis followed by post hoc Dunn's test for multiple comparisons

([c, f, i]) indicate $p < 0.0001$ after Mann Whitney's test

([d, e, g, h, j, k, l, m, n, o]) indicate p<0.0001 after Kruskal Wallis followed by post hoc Dunn's test for multiple comparisons

([p]) and ([q]) indicate $p < 0.05$ and $p < 0.001$ after Mann Whitney's test